Large size crystalline vs. co-sintered ceramic Yb 3+ :YAG disk performance in diode pumped amplifiers

Daniel Albach, Jean-Christophe Chanteloup

Large size crystalline vs. co-sintered ceramic Yb^{3+}:YAG disk performance in diode pumped amplifiers

Daniel Albach[1,*] and Jean-Christophe Chanteloup[2]

[1] *Helmholtz-Zentrum Dresden-Rossendorf, Institut für Strahlenphysik, Bautzner Landstrasse 400, 01328, Dresden, Germany*
[2] *LULI, Ecole Polytechnique, CNRS, CEA, UPMC ; Route de Saclay, 91128, Palaiseau, France*
[*] *d.albach@hzdr.de*

Abstract: A comprehensive experimental benchmarking of Yb^{3+}:YAG crystalline and co-sintered ceramic disks of similar thickness and doping level is presented in the context of high average power laser amplifier operation. Comparison is performed considering gain, depolarization and wave front deformation quantitative measurements and analysis.

OCIS codes: (140.3460) Lasers; (140.3580) Lasers, solid state; (140.3615) Lasers, ytterbium; (140.6810) Thermal effects.

References and links

1. A. Ikesue, O. Kinoshita, K. Kamata, and K. Yoshida, "Fabrication and optical properties of high-performance polycrystalline Nd:YAG ceramics for solid-state lasers," J. Am. Ceram. Soc. **78**(4), 1033–1040 (1995).
2. A. Ikesue and Y. L. Aung, "Synthesis and performance of advanced ceramic lasers," J. Am. Ceram. Soc. **89**(6), 1936–1944 (2006).
3. H. Yagi, J. Bisson, K. Ueda, and T. Yanagitani, "$Y_3Al_5O_{12}$ ceramic absorbers for the suppression of parasitic oscillation in high-power Nd:YAG lasers," J. Lumin. **121**(1), 88–94 (2006).
4. K. Ueda, J.-F. Bisson, H. Yagi, K. Takaichi, A. Shirakawa, T. Yanagitani, and A. A. Kaminskii, "Scalable ceramic lasers," Laser Phys. **15**(7), 927–938 (2005).
5. A. A. Kaminskii, M. S. Akchurin, R. V. Gainutdinov, K. Takaichi, A. Shirakava, H. Yagi, T. Yanagitani, and K. Ueda, "Microhardness and fracture toughness of Y_2O_3-and $Y_3Al_5O_{12}$-based nanocrystalline laser ceramics," Crystallogr. Rep. **50**(5), 869–873 (2005).
6. J. Akiyama, Y. Sato, and T. Taira, "Laser ceramics with rare-earth-doped anisotropic materials," Opt. Lett. **35**(21), 3598–3600 (2010).
7. T. Gonçalvès-Novo, D. Albach, B. Vincent, M. Arzakantsyan, and J.-C. Chanteloup, "14 J/2 Hz Yb^{3+}:YAG Diode Pumped Solid State Laser chain," Opt. Express **21**(1), 855–866 (2013).
8. D. Albach, J.-C. Chanteloup, and G. Touzé, "Influence of ASE on the gain distribution in large size, high gain Yb^{3+}:YAG slabs," Opt. Express **17**(5), 3792–3801 (2009).
9. D. Albach, G. LeTouzé, and J.-C. Chanteloup, "Deformation of partially pumped active mirrors for high average-power diode-pumped solid-state lasers," Opt. Express **19**(9), 8413–8422 (2011).
10. M. Arzakantsyan, N. Ananyan, V. Gevorgyan, and J.-C. Chanteloup, "Growth of large 90 mm diameter Yb:YAG single crystals with Bagdasarov method," Opt. Mater. Express **2**(9), 1219–1225 (2012).
11. M. E. Graham, B. I. Davis, and D. V. Keller, "Immersion liquids for Ruby Lasers," Appl. Opt. **4**(5), 613–615 (1965).
12. K. Ertel, C. Hooker, S. J. Hawkes, B. T. Parry, and J. L. Collier, "ASE suppression in a high energy Titanium sapphire amplifier," Opt. Express **16**(11), 8039–8049 (2008).
13. S. Guch, Jr., "Parasitic suppression in large aperture disk lasers employing liquid edge claddings," Appl. Opt. **15**(6), 1453–1457 (1976).
14. D. C. Brown, R. L. Cone, Y. Sun, and R. W. Equall, "Yb:YAG Absorption at Ambient and Cryogenic Temperatures," IEEE J. Sel. Top. Quantum Electron. **11**(3), 604–612 (2005).
15. J. Körner, V. Jambunathan, J. Hein, R. Seifert, M. Loeser, M. Siebold, U. Schramm, P. Sikocinski, A. Lucianetti, T. Mocek, and M. C. Kaluza, "Spectroscopic characterization of Yb3+-doped laser materials at cryogenic temperatures," Appl. Phys. B **116**(1), 75–81 (2014).
16. J.-C. Chanteloup, D. Albach, F. Assémat, S. Bahbah, G. Bourdet, P. Piatti, M. Pluvinage, B. Vincent, G. Le Touzé, T. Mattern, J. Biesenbach, H. Müntz, A. Noeske, and R. Venohr, "Wavelength tunable, 264 J Laser Diode Array for 10Hz/1ms Yb:YAG pumping," Fifth International Conference on Inertial Fusion Sciences and Applications (IFSA 2007), September 9–14, 2007, Kobe, Japan; J. Phys. Conf. Ser. **112**(3), 032056 (2008).

#226519 - $15.00 USD Received 7 Nov 2014; revised 22 Dec 2014; accepted 22 Dec 2014; published 9 Jan 2015

17. C. Eckert, Helmholtz-Zentrum Dresden-Rossendorf, Institut für Strahlenphysik, Bautzner Landstrasse 400, 01328 Dresden, Germany, E. Zenker, D. Albach and M. Bussmann are preparing a manuscript to be called "HASEonGPU - An adaptive, load-balanced MPI/GPU-Code for calculating the amplified spontaneous emission in high power laser media."
18. R. Wynne, J. L. Daneu, and T. Y. Fan, "Thermal Coefficients of the Expansion and Refractive Index in YAG," Appl. Opt. **38**(15), 3282–3284 (1999).
19. M. Ostermeyer, D. Mudge, P. J. Veitch, and J. Munch, "Thermally induced birefringence in Nd:YAG slab lasers," Appl. Opt. **45**(21), 5368–5376 (2006).
20. Y. Chen, B. Chen, M. K. R. Patel, and M. Bass, "Calculation of thermal-gradient-induced stress birefringence in slab Lasers," IEEE J. Quantum Electron. **40**(7), 909–916 (2004).
21. I. Shoji and T. Taira, "Intrinsic reduction of the depolarization loss in solid-state lasers by use of a (110)-cut $Y_3Al_5O_{12}$ crystal," Appl. Phys. Lett. **80**(17), 3048 (2002).
22. O. Puncken, H. Tünnermann, J. J. Morehead, P. Wessels, M. Frede, J. Neumann, and D. Kracht, "Intrinsic reduction of the depolarization in Nd:YAG crystals," Opt. Express **18**(19), 20461–20474 (2010).
23. E. A. Khazanov, "Thermally induced birefringence in Nd:YAG ceramics," Opt. Lett. **27**(9), 716–718 (2002).
24. A. Lucianetti, D. Albach, and J.-C. Chanteloup, "Active-mirror-laser-amplifier thermal management with tunable helium pressure at cryogenic temperatures," Opt. Express **19**(13), 12766–12780 (2011).

1. Introduction

Progress in recent years in ceramic laser gain media [1] triggered a particular interest within the Diode Pumped Solid State Laser (DPSSL) community for new gain media with improved performances and/or characteristics. Not only can ceramics be manufactured in potentially any shape and large dimensions, but also new structures are accessible due to the versatility of ceramics, like rooftops, composite rods and co-doped absorber claddings [2, 3].

Co-sintered ceramics exhibit regions with a different doping ion or different doping concentration. This is especially beneficial due to the significant reduction of Amplified Spontaneous Emission (ASE) and/or deleterious thermal effects. This approach is typically found in Anti-ASE-caps or covers with a higher thermal conductivity in order to transport the heat into a heat sink more efficiently. Another interesting property of laser ceramics is their potentially better fracture toughness, as cracks tend to stop at grain boundaries, while the thermal conductivity is not much different from their crystalline counterpart when produced through specific manufacturing processes [4, 5].

Most of the laser quality ceramics are restricted to the cubic lattice system. Prominent cases are especially rare-earth doped Yttrium Aluminum Garnet (YAG) ceramics. Recent results have successfully demonstrated the production of non-cubic ceramics, like Fluoro APatite (FAP), by applying strong magnetic fields during sintering [6]. Materials difficult to grow as a single crystal, e.g. sesquioxides due to their high melting temperature, are interesting candidates for ceramic laser gain media as well.

For high energy lasers, ceramics are potentially attractive candidates due to their large size, as laser damage is one of the restricting factors when scaling laser gain media. Typical laser damage thresholds for nanosecond pulses are found to be in the order of 3 J/cm^2 in the near infra-red to ensure a reliable laser operation. Consequently, large laser gain media with diameters in the size of more than 5 cm clear aperture are needed to sustain pulsed laser energies of more than 100 J.

The Lucia laser system, currently under development at the Laboratoire pour l'Utilisation des Laser Intenses (LULI) at the Ecole Polytechnique, France, aims for pulse energies significantly above 10 J in the ns-pulse regime. Lucia is an Yb^{3+}:YAG based Master-Oscillator Power-Amplifier (MOPA) DPSSL described in [7]. Amplifying stages rely on the active mirror principle where the gain medium disk is cooled through an HR coated surface, while pump and extraction take place through the opposite AR coated surface.

Influence of ASE on the gain distribution within such large size, high gain Yb^{3+}:YAG slabs has already been described [8]. Thermally induced wave front distortions generated by Lucia main amplifier disk were detailed as well [9]. After describing the experimental samples (section 2) and giving comparative gain measurements (section 3), this paper focuses on the experimental cross evaluation of wave front distortion (section 4) and thermally

#226519 - $15.00 USD Received 7 Nov 2014; revised 22 Dec 2014; accepted 22 Dec 2014; published 9 Jan 2015

induced depolarization loss (section 5) introduced by crystal and ceramic Yb^{3+}:YAG disks when submitted to the significant heat load experienced in the high average-power active-mirror amplifier of the Lucia DPSSL.

2. Experimental platform

Experimental cross evaluations of wave front distortions and depolarization were performed on the Lucia room-temperature water cooled main amplifier head [7] with two 7 mm thick, 2 at.% Yb^{3+} doped YAG disks as shown in Fig. 1. The first one is a 60 mm diameter single crystal grown using Horizontal Direct Crystallization [10] by Laserayin, CSC, Yerevan, Armenia. The second disk is a co-sintered ceramic where the Yb^{3+} doped 35 mm diameter central part is surrounded by a 5 mm wide 0.25 at.% Cr^{4+} doped periphery. It was manufactured by Konoshima Ltd., Japan.

For operation near room temperature, index matching liquids are a solution of choice to reduce the reflectivity at lateral surfaces. For this work, water was circulating in contact with the cylindrical surface of the disk. Liquids like α-bromonaphtalene (n = 1.66) or diiodomethane (n = 1.74) [11, 12] offer a better index matching to YAG (n = 1.82) compared to water (n = 1.33). But neither of these fluids revealed any compelling benefit over water in our experimental case, as the main contribution to parasitic rays feedback into the gain medium was due to the disk's mount.

A low reflectivity treatment, black Nickel [13], was applied to the inner part of the disk mount facing the YAG lateral edges. The resulting low reflectivity helped to significantly reduce feedback back into the laser gain medium.

Foreseen low temperature (<200K) operation of the 2nd Lucia power amplifier prohibits the use of liquids due to temperature considerations. Cr^{4+} doped YAG can actually easily absorb this emission at 1030 nm, as is depicted in Fig. 1. We measured an absorption of 5.5 cm^{-1} for a doping level of 0.25 at.%. Processing a disk shaped crystal of more than 10 cm^3 with such ring structure would be technically challenging. Fortunately, ceramic *co-sintering* is a manufacturing process offering the possibility to obtain such composite structure, as depicted in Fig. 1.

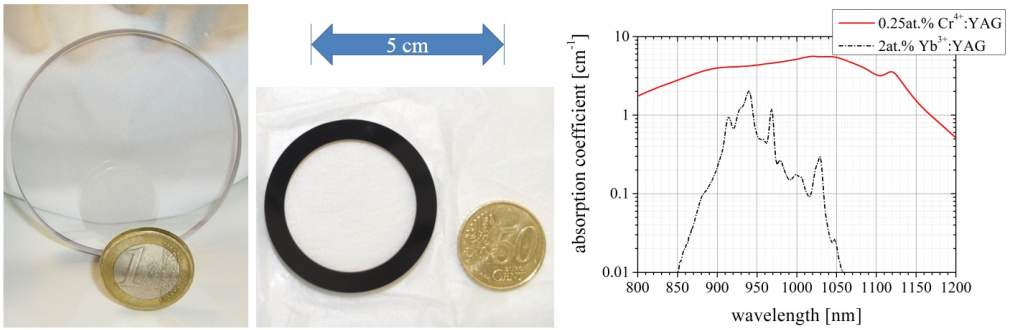

Fig. 1. 7 mm thickness, 2 at.% Yb^{3+} doped YAG disks in crystalline form (left, 60 mm diameter) and in ceramic form (center, 45 mm diameter including a 5 mm wide 0.25 at.% Cr^{4+} doped periphery). The horizontal double head arrow indicates the pictures common scale. Yb^{3+}:YAG and Cr^{4+}:YAG absorption spectra are depicted on the right graph.

3. Small signal gain performance

Due to the temperature dependency of laser gain media cross sections [14,15], only a Small Signal Gain (SSG) measurement under single shot condition is a viable way to determine the impact of gain medium structure on ASE feedback. Despite the fact that the reflectivity of the outer gain medium mount was strongly reduced by applying a black Nickel coating and avoiding any parallel surfaces to the gain medium, reflections from the YAG/water surface still exist. Omitting residual reflections from the mount, about 2% reflectivity from the

#226519 - $15.00 USD Received 7 Nov 2014; revised 22 Dec 2014; accepted 22 Dec 2014; published 9 Jan 2015

crystal/water interface still remains. In the case of the composite ceramic, all feedback can be omitted thanks to Cr^{4+} absorption. The test setup is sketched in Fig. 2. The collimator exit port of a 15 mW fiber coupled cw laser at 1029.8 nm is imaged onto the backside of the HR coated gain medium and then imaged onto a photodiode (Thorlabs DET36). The beam diameter is about 1 mm.

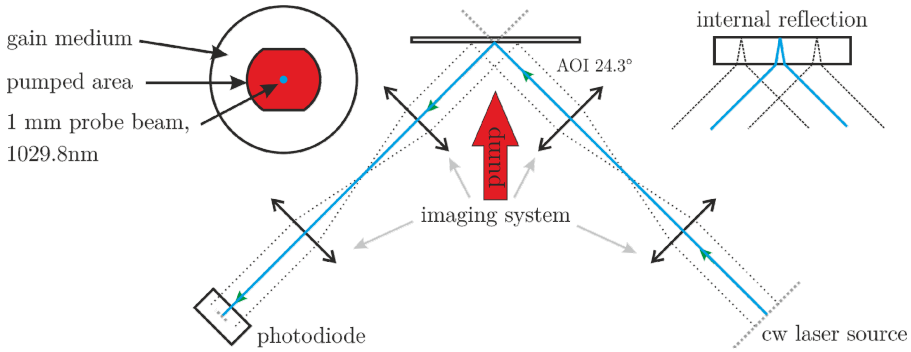

Fig. 2. The small signal gain (SSG) measurement setup. A cw laser source is imaged onto the backside of the laser gain medium and is again imaged onto a photodiode. Out of the oscilloscope traces the SSG is calculated.

As pump source, the Lucia main amplifier diode array was used [16]. 41 laser diode stacks, each emitting up to 3 kW peak power in 1 ms long pulses at 940 nm, are guided on a 7 cm^2 aperture. This aperture consists of a circular aperture of 30 mm limited in height to 24 mm by guiding mirrors [9]. We reach up to 16 kW/cm^2 on average over the whole surface. Due to the light concentration system, we have a 15% higher intensity in the center due to modulations from the individual laser diode stacks - about 18.7 kW/cm^2 when driven at the highest diode current of 150 A.

Figure 3 (left) shows the resulting SSG at 16 kW/cm^2 for the crystal, the composite ceramic, a simulation taking ASE into account and a simulation without taking ASE into account. The simulation is performed using the HASEonGPU code [17] which includes reflection on front and back surface as well as the spectra of emission and absorption cross sections. Peripheral surfaces are treated as perfectly absorbing in this code.

Starting at ~600 µs pump duration, ASE has to be taken into account for the samples under test. From this point, crystal and ceramic SSG curves start diverging due to feedback from the periphery. In the case of a 30 mm diameter pumped area and a thickness of 7 mm, Total Internal Reflection (TIR) guided reflections will undergo ~7.4 reflections in average while passing through the pumped area. With an Angle Of Incidence (AOI) close to 33°, the length between each reflection is ~20% longer than the thickness of the gain medium. We have to keep in mind, that in the crystalline case additional ~30 mm of non-pumped Yb^{3+}:YAG have to be crossed for each roundtrip between the peripheral surfaces leading to a transmission of about 33% for 2 at.% doped YAG at room temperature. A reflectivity of the periphery of about 2% to 3% finally corresponds to measured SSG values in the range of 3 to 3.4. Despite being a very simplified approximation, it is in very good agreement with the experimentally found starting point of major differences between the SSG for composite ceramic and the crystal.

As a comparison of ceramic and crystal SSG performance, Fig. 3 (right) shows the SSG values of the crystal versus the ceramic under similar pump intensities at 940 nm over 1 ms duration. SSG values significantly larger than 3 show increased losses for the crystalline case. This finally results in a 20% difference for the highest pump intensities available. The diverging behavior occurs at pump intensities close to 12 kW/cm^2.

#226519 - $15.00 USD Received 7 Nov 2014; revised 22 Dec 2014; accepted 22 Dec 2014; published 9 Jan 2015

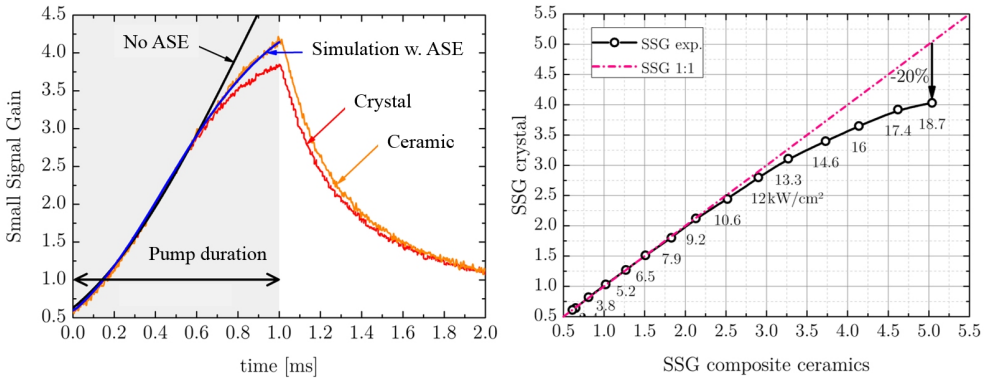

Fig. 3. Left: ASE performance / SSG of the crystal (red), ceramic (orange), the case of no ASE (black), simulation with ASE (blue). Greyed part shows the pump duration (also indicated by the arrow). Right: SSG of the crystal compared to the SSG of the composite ceramics. The dash-dot line indicates SSG parity. The numbers indicate the average pump intensity in kW/cm^2.

4. Thermally induced focal lengths

The active mirror architecture leads to a parabolic temperature distribution along the thickness of the homogeneously doped YAG disk, since the HR coated side is in contact with a coolant, while the other side is not actively cooled. The associated heat exchange coefficient h_{air} is several orders of magnitude weaker compared to the $h_{coolant}$ coefficient measured in our setup to be 15 kW/m^2/K. The resulting temperature difference between the front and back side leads to the bending of the disk as illustrated in Fig. 4. The active mirror can therefore be seen as a convex mirror, where an incoming beam with a flat wave front will exit the amplifier as a divergent beam. Let us call f_{mech} the associated focal length.

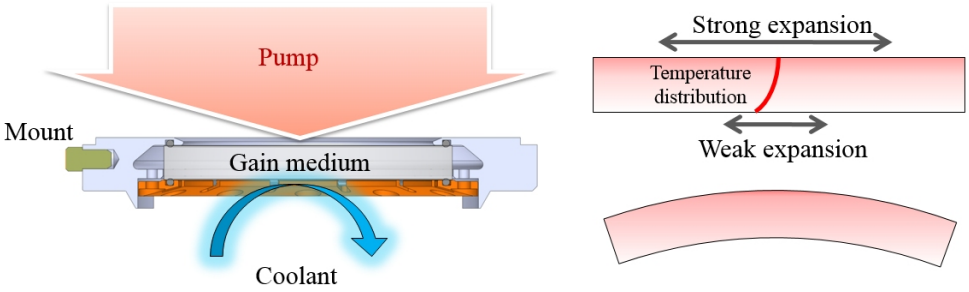

Fig. 4. Lucia water cooled power amplifier mount (left) hosting the 7 mm YAG disk pump from the top and cooled from the other side. Thermally induced differential surfaces expansion (top right) leads to the disk bending (bottom right).

However, the thermally induced mechanical bending is not the only phenomenon encountered. In the case of a disk which is fully pumped over its whole surface no radial temperature gradients are expected. However, only a limited portion of the whole front surface is under pump action, and consequently a radially varying temperature distribution will appear [10]. In the case of the composite structure of the ceramic gain medium, additional absorption of ASE will take place in the chromium doped external ring. We therefore expect a completely different temperature distribution compared to the crystalline gain medium.

With a thermal coefficient refractive index change dn/dT being positive [18] for YAG, a positive thermal lens f_{therm} partially compensates for the concave active mirror in the case of the crystal [9]. The global focal length f_{Tot} satisfies Eq. (1) where f_{mech} contributes half as

#226519 - $15.00 USD Received 7 Nov 2014; revised 22 Dec 2014; accepted 22 Dec 2014; published 9 Jan 2015

much as f_{therm} since the thermal lens is encountered before and after reflection on the convex HR surface.

$$f_{Tot.} = \frac{f_{mech.} f_{therm.}}{2 f_{mech.} + f_{therm.}} \quad (1)$$

In the case of the ceramic f_{therm} is almost absent while f_{mech} is strongly increased due to the higher thermal load. Figure 5 confirms that the chromium periphery creates a hot ring due to its strong parasitic transverse rays energy absorbing role. This phenomenon does not take place in the crystal case since these rays are refracted into the peripheral circulating water and absorbed by the 2% reflecting mount (itself cooled with water). Taking into account that, in any case, all the light trapped by TIR will ultimately be absorbed in the Cr^{4+} cladding, one can estimate that an important amount of the pump power will be transformed into an additional heat source in the cladding. Calculations with our ASE code show about 40% heat load in the cladding.

Relying on the experimental set-up described in [9], wave front measurements were performed with both disks over a large range of incident pump powers. Out of the wave front maps the thermally induced defocus components were derived using the Zernike polynomials. The corresponding calculated focal lengths are illustrated in Fig. 6. This experimental data confirms the compensation effect of f_{therm} and f_{mech} in the case of the crystal where the global focal length never exceeds 100 m even in the half kilowatt average power regime. We observe that f_{Tot} is degraded due to the increased thermal load for the ceramic. More than one order of magnitude is revealed compared to the self-compensated crystal case.

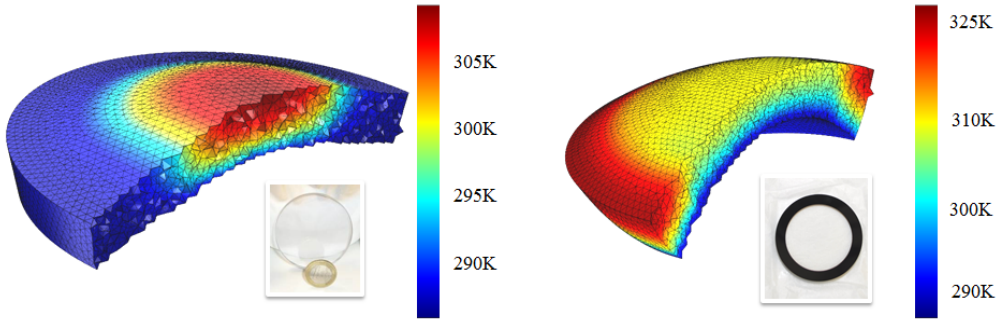

Fig. 5. 3D thermo-mechanical model of both crystal (left) and co-sintered ceramic (right) 7 mm thick YAG disks. 15 kW/m^2/K heat exchanged coefficient water cooling takes place from the bottom (observe the cold blue surface) while pumping occurs on the top surface. The color temperature distribution clearly reveals the opposite radial temperature gradient of both cases. The heat source corresponds to a 16 kW/cm^2 pumping at 2 Hz, 1 ms.

#226519 - $15.00 USD Received 7 Nov 2014; revised 22 Dec 2014; accepted 22 Dec 2014; published 9 Jan 2015

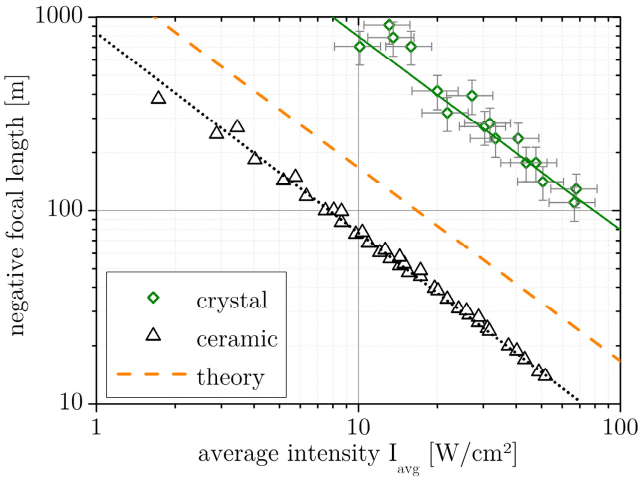

Fig. 6. Global thermally induced negative focal length f_{Tot} versus average pump intensity for the crystal (diamonds) and the ceramic (triangles). The dashed line corresponds to the theoretical focal length [9]. The relative error bars for the ceramic case are in the same order as for the crystal. They were omitted for visibility reason.

5. Depolarization measurements

In order to fully study thermally induced consequences on the extraction beam quality, not only its wave front perturbations need to be evaluated. The way its polarization quality might be affected is also a key aspect. This has a considerable impact on the Lucia amplifying stage to stage isolation with polarization dependent devices like Pockels cells or Faraday rotators. The efficiency of foreseen frequency conversion will also be strongly dependent of the polarization quality of the amplified pulses.

5.1 Depolarization losses

Cubic materials, like Yb^{3+}:YAG, do not show any directional preference of the refractive index in the ideal, i.e. stress-less, case, it will become non-isotropic when stress is applied [19, 20]. In the case of a laser gain media, the average pump power generates an average heat source leading to thermal expansion, and therefore stress. Such stress can add up and lead to depolarization losses so high, that laser operation will generate laser beams with a significant portion of energy in unintended states of polarization within the beam. On top of this, intrinsic stress within the material due to the manufacturing process will also contribute to depolarization losses even in the case of an un-pumped gain medium. For crystalline gain media, the orientation of the unit cell is therefore important, as it is shown in Fig. 7. For cubic crystalline laser gain media, the [111] orientation is the most interesting, as a rotation around its axis has no influence on depolarization losses, as long as the angle of incidence is 0°. For angles significantly larger than 0°, a 120° symmetry is found, as it is shown in Fig. 7. As one can imagine, other crystal axis orientations will result in a different pattern when turning around this particular axis. For cubic YAG, an orientation along [100] can potentially minimize depolarization losses [21, 22], but this effect is very sensitive to misalignment. Other orientations may not find rotational dependent losses less than the [111] orientation and thus are a somehow bad choices (e.g. [110] in our setup).

#226519 - $15.00 USD Received 7 Nov 2014; revised 22 Dec 2014; accepted 22 Dec 2014; published 9 Jan 2015

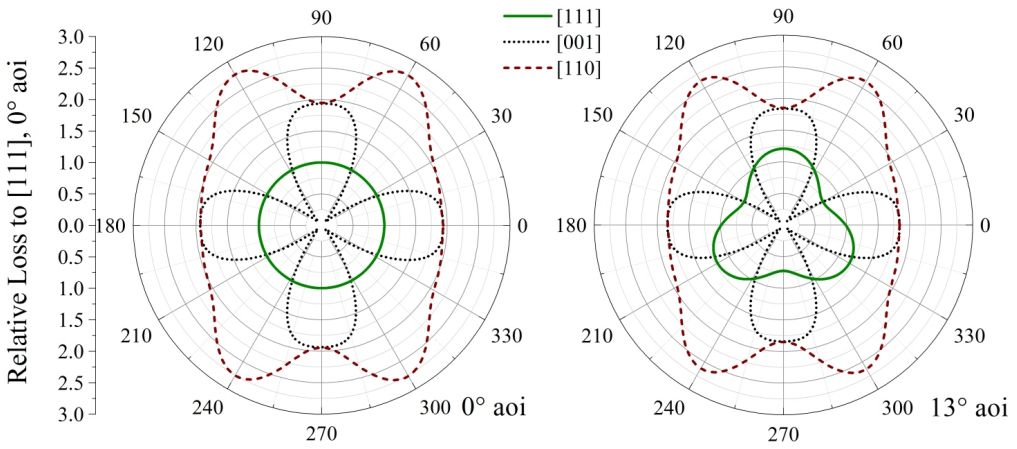

Fig. 7. Calculated angular depolarization loss maps for an Yb^{3+}:YAG crystal carrying three type of orientations. The left map is obtained for a double pass (active mirror architecture) extraction beam propagating through the disk at normal incidence (AOI 0°) whereas a 13° AOI (corresponding to Lucia experimental case) is depicted on the right map.

For ceramic media the situation is somewhat different. Due to the random nature of the orientation of each subpart of the ceramic, no orientation dependence is expected, except maybe stresses induced due to coating, mounting, and other non-symmetric influences. The depolarization pattern is independent of crystal rotation and is in the same order as for a crystal in [111] configuration under 0° [23].

As already mentioned in the previous section, ASE simulations of our co-sintered ceramics showed, that we can expect about 40% of the total pump power ultimately ending in the ceramic cladding. This additional heat source significantly increases the deformation and stress compared to the crystalline case, where ASE rays are basically allowed to freely exit the gain medium and be dumped in the specially designed peripheral cavity filled with water.

5.2 Experimental setup

A dedicated experimental bench was set up as shown in Fig. 8: a 50 mW cw laser source at 1064 nm was polarized and transformed into an almost flat top beam using a beam expander and a serrated aperture of 22 mm outer diameter. This image plane was image relayed onto the HR-coated backside of the gain medium using a telescope with a slight magnification resulting in a beam diameter of 24 mm. The beam was then imaged onto a CCD camera while passing through a rotating analyzer as well as a set of optical densities OD and two 1064 nm bandpass filters (Thorlabs FL1064-10). By carefully calibrating 2"x2" optical densities using a Varian Cary 500 UV-VIS spectrometer, an extinction ratio of $2x10^{-5}$ averaged over the whole beam was obtained when observed between crossed polarizers (Altechna, Glan-Laser type) while replacing the gain medium with a silver mirror. The gain medium was then carefully inserted into its holder and aligned into the test beam line. The gain medium mount could be rotated over 360°. The extraction beam angle was 24.3°, corresponding to a 13° propagation angle within the gain medium. The overall detection limit of this set-up is 0.02% average depolarization loss.

With a test wavelength of 1064 nm sufficiently close to the design wavelength of the optical coatings, interference patterns were not visible, while the bandpass filter allowed blocking the spontaneous emission around 1030 nm.

The Lucia main amplifier diode array was used as the pump source (see section 3). Guiding this pump light [9] through a circular aperture of 30 mm diameter led to about 110 J available for the gain medium. Considering the beam overlap including reflection on the HR

#226519 - $15.00 USD Received 7 Nov 2014; revised 22 Dec 2014; accepted 22 Dec 2014; published 9 Jan 2015

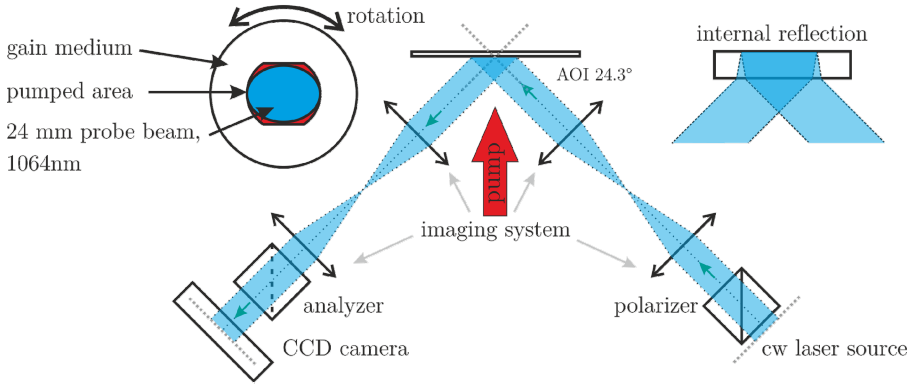

Fig. 8. The experimental setup for the measurement of depolarization loss. A polarized cw laser beam is imaged onto the backside of the HR coated laser gain medium and recorded by a CCD camera setup. By rotating of the analyzer relative to the polarizer the depolarization loss can be measured. The gain medium can be rotated as well.

coated side (see top right insert of Fig. 8), a circular beam diameter of 24 mm left sufficient space for alignment, while filling most of the pumped aperture and avoiding clipping at the gain medium mount. In order to adjust the average power on the target, we relied on the driving current of the laser diodes and/or the repetition rate of the laser diode drivers. Pump laser wavelength shift for the different average power regimes is controlled by applying a constant bias current on the laser diode stacks of up to 1 A, which is far below the lasing threshold of about 15 A [16]. Using this method we ensured that laser diode emission wavelength drifts did not affect the average absorbed pump power.

5.3. Experimental results

Both crystal and ceramic were rotated around the axis perpendicular to the front surface. For an average intensity of 40 W/cm^2 in single pass, a strong modulation appears on the crystal angular depolarization loss map (see red triangles, right map of Fig. 7). The four-leaf symmetry observed is unexpected for a [111] oriented crystal. It was later discovered that this specific crystal was actually incorrectly oriented during post-manufacturing process, its orientation being about 10° to [110].

As expected, rotating the ceramic revealed almost no impact on depolarization loss. Left graph of Fig. 9 illustrates the increasing (% in log scale) losses (single pass) experimentally recorded when ramping up the average pump brightness at the gain medium level. Below 20 W/cm^2, only intrinsic birefringence combined with potential mounting stress-induced birefringence can be observed. When increasing the brightness, the depolarization loss becomes proportional to I_{avg}^2 before ultimately reaching saturation. The quadratic behavior is indicated by the dashed lines in the Fig. 9 (left). At 40 W/cm^2, we observe that the 1% loss value is already exceeded for the co-sintered ceramic while it stays 5 times lower for the crystal when oriented at one of the four optimum angles. When doubling the pump average power to reach 80 W/cm^2, losses greater than 5% over the beam full aperture are recorded.

Yb^{3+}:YAG cross sections are not sensitive to polarization. But the angular multiplexing extraction architecture in place on a laser chain like Lucia generates differential losses on the s and p polarizations after each reflection on optics oriented at non-normal incidence. This is obviously the case of the YAG disk (24°) but also for several mirrors (45° or 30°). Although special care is given to the optimization of the dielectric layers to minimize reflection losses, it is still not zero. Some applications of the amplified pulse train require frequency conversion. The involved non-linear processes are generally characterized by an efficiency strongly related to the polarization quality of the IR beam to be converted. Consequently, controlling the state of polarization of the amplified pulses appears mandatory.

#226519 - $15.00 USD Received 7 Nov 2014; revised 22 Dec 2014; accepted 22 Dec 2014; published 9 Jan 2015

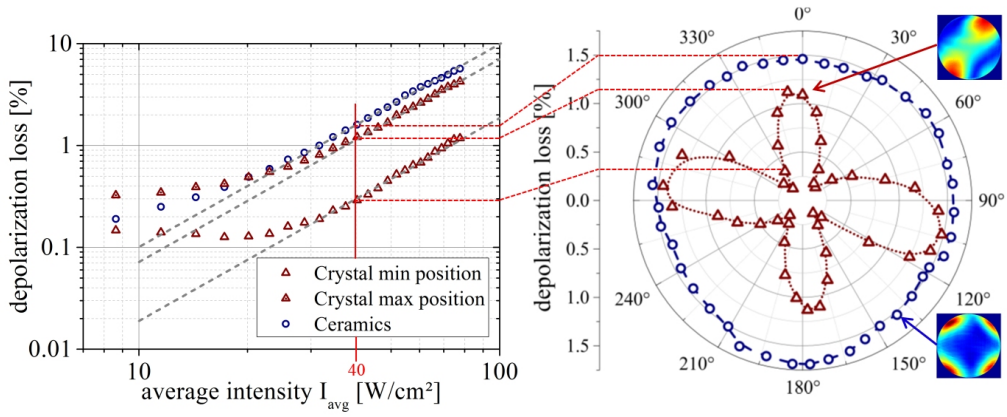

Fig. 9. Birefringence loss for the ceramic (blue circles) and the crystal (red triangles). For both diagrams the vertical scales give losses in % with respect to the incident energy beam. The evolution of the average pump intensity hitting the disks is depicted on the left logarithmic diagram while the right angular map is given for a 40W value. The dashed lines in left the graph indicate a quadratic behavior of the depolarization loss with increasing average intensity.

6. Conclusions

A comprehensive experimental benchmarking of Yb^{3+}:YAG disks of similar thickness and doping level was performed with the Lucia MOPA DPSSL active mirror water cooled amplifier head. The differences of both samples under study were the nature of the host YAG matrix (ceramic vs crystal) as well as the radial dimension and structure of the disk.

Whereas the 60 mm crystalline disk was supplied specifically for such operating environment (300 K) where ASE parasitic rays mitigating can be at least partially handled with a peripheral circulation of water, the co-sintered ceramic was designed to be used at a much lower temperature (<200 K) where parasitic rays absorption takes place in the Cr^{4+} doped surrounding ring.

This study focuses on the two thermally induced major consequences on an amplified beam: its wave front deformation (quantified here with the defocus) and depolarization. This work reveals a clear advantage in favor of the crystal. Its monolithic structure contributes largely to this conclusion. Indeed the accumulation of heat in the periphery of the composite ceramic puts it in considerably more intense thermally-induced stress situation than the crystal YAG disk. This is quantified by an order of magnitude difference in term of global thermal lens in our cases.

Moreover, due to its anamorphous nature the ceramic is revealed to be much more sensitive to thermo-mechanical stresses. This is observed when comparing both disks ability to maintain the polarization quality of the beam to be amplified.

Following these observations, and considering the fact that there is no practical alternative to co-sintered ceramics for the Lucia low temperature operated 2nd amplifier head, a new generation of composite ceramics have been ordered. The Cr^{4+} doping level has been divided by 10 to reach 0.025 at%, allowing then the parasitic rays energy to be spread much deeper in the outer ring. Consequently, the thickness of this cladding layer was increased. Such approach should help avoiding the heat load to be concentrated at the Yb^{3+}/Cr^{4+} interface and therefore relaxing somehow the internal constraints. Also, a cooling approach minimizing radial gradients will be implemented [24]. On the other hand the efficiency of Cr^{4+} cladding for ASE mitigation was revealed through gain measurements.

Acknowledgments

The research leading to these results has received funding from LASERLAB-EUROPE (grant agreements no. 228334 and n° 284464, EC's Seventh Framework Programme).

#226519 - $15.00 USD Received 7 Nov 2014; revised 22 Dec 2014; accepted 22 Dec 2014; published 9 Jan 2015